A DIFFERENTIAL APPROACH FOR RAIN FIELD TOMOGRAPHIC RECONSTRUCTION USING MICROWAVE SIGNALS FROM LEO SATELLITES

Xi Shen[⋆] *Defeng (David) Huang*[⋆] *Claire Vincent*[†] *Wenxiao Wang*[⋆] *Roberto Togneri*[⋆]

[⋆] Department of Electrical, Electronic and Computer Engineering,
The University of Western Australia, Australia
[†] School of Earth Sciences, The University of Melbourne, Australia

ABSTRACT

A differential approach is proposed for tomographic rain field reconstruction using the estimated signal-to-noise ratio of microwave signals from low earth orbit satellites at the ground receivers, with the unknown baseline values eliminated before using least squares to reconstruct the attenuation field. Simulations are done when the baseline is modelled by an autoregressive process and when the baseline is assumed fixed. Comparisons between the reconstruction results for the differential and non-differential approaches suggest that the differential approach performs better in both scenarios. For high correlation coefficient and low model noise in the autoregressive process, the differential approach surpasses the non-differential approach significantly.

***Index Terms*—** rain field, 3-D tomography, LEO, SNR estimation, differential method

1. INTRODUCTION

Using microwave attenuation measurements for rainfall monitoring has received much attention in the past few decades. It is becoming increasingly promising recently due to mainly two reasons. Firstly, a large number of microwave communication systems such as commercial wireless communication networks (CWCNs) [1] and satellite-to-ground networks are in operation, and they provide off-the-shelf attenuation data for rainfall monitoring. Secondly, most of these communication systems use Ku-band ($12 \sim 18$ GHz) or Ka-band ($26.5 \sim 40$ GHz). Signals in these bands are sensitive to rain attenuation, which in turn indicates that such communication links are suitable for rainfall monitoring.

Both CWCNs and geostationary earth orbit (GEO) satellite systems offer stationary microwave links. Many studies have confirmed that these links can be used as a means of real-time 2-D rainfall reconstruction [2–4]. The hypothesis of using low earth orbit (LEO) satellite microwave links for three-dimensional (3-D) rain field tomography was first proposed by Huang *et al.* in 2016 [5], in which moving microwave links were investigated for the purpose of rainfall estimation. Similar to the motion of the signal source in computed tomography (CT) [6], the rotational motion of the LEO satellites makes it possible to perform 3-D tomographic reconstruction of rain fields. In [7], Shen *et al.* have shown that vertical rain fields can be reconstructed from the received signal level (RSL) measurements of multiple receivers. The approach of using the estimated signal-to-noise ratio (SNR) at the ground receivers for LEO satellites to achieve 3-D tomographic rain field reconstruction was analyzed in detail in [8].

For both CWCNs and satellite systems, the path-integrated rain attenuation is obtained indirectly through the observations of SNR or RSL for the microwave links. In the CWCNs method, the baseline that includes attenuation from all sources except the rain needs to be carefully evaluated [9]. By contrast, using microwave signals from LEO satellites with the method described in [8], the unknown baseline for one pass was easily solved by a set of equations that are formed along the movement of the LEO satellites. However, the key assumption in [8] was that the baseline remains constant within one pass of the satellite.

There are three issues with the above assumption. First, the gain of the Radio Frequency (RF) chains and antennas, which is part of the baseline, could change during one pass of the satellite [10]. Second, the effect from other attenuation sources such as water vapor may also change along with the movement of the communication link [11]. Third, in the practical scenario where a LEO satellite constellation for global Internet services is used, one receiver often needs to communicate with multiple satellites to ensure seamless handover [12], with each satellite corresponding to an unknown baseline. This means that more unknowns need to be introduced in the model of [8], leading to degraded rain field reconstruction performance.

In this paper, we propose a new differential approach in the reconstruction process for the same LEO satellite signal attenuation model as that in [8]. To minimize the effect of the three issues mentioned above, the proposed approach differentiates two equations of adjacent samples to eliminate the unknown baseline before using least squares to retrieve the specific attenuations. Moreover, in contrast to [8], where only

rainwater was considered, we consider a synthetic attenuation field that takes into account rainwater, cloud water and melting hydrometeors in the atmosphere. Simulations are carried out with the baseline modelled by a first-order autoregressive (AR(1)) process and also with fixed baseline. Comparisons suggest that the differential approach offers a better reconstruction outcome than the non-differential approach.

2. SYSTEM MODEL

The signal attenuation model used here is the same as that in [8]. Consider a LEO satellite passes over the rain event of interest, and the satellite has direct spot beam links to all ground receivers. Suppose that there are M signal samples available at the receiver. For the k-th sample, the receiver's SNR $\rho(k)$ in decibels is given by:

$$\rho(k) = C(k) - F_n(k) - A_R(k) - A_F(k) \,, \qquad (1)$$

$$k = 1, 2, \cdots, M,$$

where $A_R(k)$ and $A_F(k)$ are the rain attenuation and the free space path loss, in decibels, respectively. The unknown parameter $C(k)$ is related to the noise temperature of the receiving system $T_{sys}(k)$ as follows:

$$C(k) = 10 \cdot \log \frac{\xi_C(k) \cdot P_t(k)}{k_B \cdot B \cdot T_{sys}(k)} \,, \qquad (2)$$

where k_B is the Boltzmann constant, B is the bandwidth of the communication system, $P_t(k)$ is the power of the transmitted signal at the satellite and $\xi_C(k)$ represents the channel gain due to all other factors such as the gain of the RF chains and effects of water vapor. Essentially, term $C(k)$ represents a baseline value for a receiver, which is mainly determined by the noise temperature of the receiving system, the RF gain and the power of the transmitted signal.

The noise figure $F_n(k)$ is related to $T_{sys}(k)$ and the sky temperature $T_{sky}(k)$ as follows:

$$F_n(k) = 10 \cdot \log(\frac{T_{sys}(k) + T_{sky}(k)}{T_{sys}(k)}) \,. \qquad (3)$$

Note that $F_n(k)$ only depends on the sky temperature $T_{sky}(k)$ if the system temperature $T_{sys}(k)$ is known. In this model, rain is the primary source for $T_{sky}(k)$, which is generally given by [13]:

$$T_{sky}(k) = \frac{\int\limits_{\Omega} G(k,\Omega) T(\Omega)\, d\Omega}{\int\limits_{\Omega} G(k,\Omega)\, d\Omega} \,, \qquad (4)$$

where $G(k,\Omega)$ is the antenna gain pattern and $d\Omega$ is the solid angle. $T(\Omega)$ is the noise temperature for a particular direction, which is given by (for time k):

$$T(k) = t_m(1 - 10^{-\frac{A_R(k)}{10}}) \,, \qquad (5)$$

where t_m is the mean path temperature, in Kelvin, and A_R is the total path rain attenuation for that direction, in dB. We assume that the beam pattern of the antenna is known so the relation between $T_{sky}(k)$ and $A_R(k)$ can be established using Eqs. (4) and (5).

Meanwhile, $A_F(k)$ is a function of the satellite-to-ground path length L_S and the signal frequency f, and is commonly given by [14]:

$$A_F(k) = 20 \cdot \log(L_S(k)) + 20 \cdot \log(f) + 92.45 \,, \qquad (6)$$

where the unit of $L_S(k)$ is in km and f in GHz.

Since $A_F(k)$ can be regarded as known, Eq. (1) indicates that $A_R(k)$ can be obtained from the SNR estimation as follows:

$$A_R(k) = C(k) - \hat{\rho}(k) - A_F(k) - F_n(k) \,, \qquad (7)$$

where $\hat{\rho}$ is the estimated SNR at the receivers.

3. THE DIFFERENTIAL APPROACH

The space of interest is divided into multiple voxels. The relation between the path-integrated rain attenuation and the specific rain attenuation in each voxel is given by (see [8] for details):

$$A_R(k) = \sum_{j=1}^{N} a_j l_{k,j} \,, \qquad k = 1, 2, \cdots, M, \qquad (8)$$

where a_j is the specific rain attenuation (in dB/km) in the jth voxel, and $l_{k,j}$ is the length of the signal link in the same voxel for the k-th sample. Using Eq. (8), we can rewrite Eq. (7) as follows:

$$\sum_{j=1}^{N} a_j l_{k,j} - C(k) = -\hat{\rho}(k) - A_F(k) - F_n(k) \,. \qquad (9)$$

For an adjacent signal sample $k+1$:

$$\begin{aligned} &\sum_{j=1}^{N} a_j l_{k+1,j} - C(k+1) = \\ &- \hat{\rho}(k+1) - A_F(k+1) - F_n(k+1) \,. \end{aligned} \qquad (10)$$

As the two samples are close in time, the difference between $C(k+1)$ and $C(k)$ can be ignored for good approximation. Subtracting Eq. (9) from Eq. (10) to eliminate C, we have

$$\sum_{j=1}^{N} a_j (l_{k+1,j} - l_{k,j}) = Y_k \,, \qquad (11)$$

where Y_k can be simplified to (using Eqs. (6) and (3)):

$$\begin{aligned} Y_k = \hat{\rho}(k) - \hat{\rho}(k+1) + 20 \cdot \log \frac{L_S(k)}{L_S(k+1)} \\ +10 \cdot \log \frac{T_{sys} + T_{sky}(k)}{T_{sys} + T_{sky}(k+1)} \,. \end{aligned} \qquad (12)$$

For $k = 1, 2, \cdots, M-1$, we rewrite Eq. (11) as:

$$\mathbf{L} \cdot \alpha = \mathbf{Y} \,, \tag{13}$$

where $\mathbf{L} =$

$$\begin{bmatrix} l_{2,1} - l_{1,1} & l_{2,2} - l_{1,2} & \cdots & l_{2,N} - l_{1,N} \\ l_{3,1} - l_{2,1} & l_{3,2} - l_{2,2} & \cdots & l_{3,N} - l_{2,N} \\ \vdots & \vdots & \vdots & \vdots \\ l_{M,1} - l_{M-1,1} & l_{M,2} - l_{M-1,2} & \cdots & l_{M,N} - l_{M-1,N} \end{bmatrix}$$

and

$$\alpha = [a_1 \; a_2 \; \cdots \; a_N]^T \,, \; \mathbf{Y} = [Y_1 \; Y_2 \; \cdots \; Y_{M-1}]^T$$

Note that the differential approach requires the differential distance matrix $\mathbf{L}$. If the grid is predefined and the trajectory of the satellite is given, $\mathbf{L}$ can be calculated offline and regarded as known. However, vector $\mathbf{Y}$ requires $T_{sky}(k)$, which can not be regarded as known because no *a priori* knowledge of the rain field is assumed available. Hence we use the same iterative algorithm proposed in [8] to iteratively update the value of $T_{sky}(k)$ and thus the differential vector $\mathbf{Y}$.

For the first iteration T_{sky} is set to be zero. Given Y_k, we solve α by formulating the following linear least-squares problem:

$$\hat{\alpha} = \mathbf{arg\ min}\; S(\alpha) \,, \tag{14}$$

subject to

$$a_j \geq 0 \,, 1 \leq j \leq N \,,$$

where

$$S(\alpha) = ||\mathbf{Y} - \mathbf{L} \cdot \alpha||^2 \,. \tag{15}$$

After the first iteration, α has been retrieved. Consequently, T_{sky} can be updated using Eqs. (5) and (4), and then vector $\mathbf{Y}$ can be updated using Eq. (12). The following iterations will utilize the updated $\mathbf{Y}$ and apply the same least-squares method to achieve a better estimation of α.

4. SIMULATION RESULTS

To test the performance of the differential reconstruction approach, a synthetic attenuation field is employed from the simulation of a single convective storm near the Great Barrier Reef using the WRF model. It is a 20 by 15 grid point (grid-length 1.33 km) subset of a larger simulation covering the southern part of the Great Barrier Reef and adjacent coastline. The lowest 50 vertical levels (below about 6.2 km) are considered, and the rainwater, cloud water and melting hydrometeors are all taken into account for the attenuation field. For rainwater, the same method employed in [8] is used, where the rainwater mixing ratio (in g/kg) is firstly converted to rainfall rate (in mm/h), and then a linear $K - R$ relation is assumed to generate the rain attenuation field (in dB/km). The melting layer forms the second part of the attenuation field. The total mixing ratios of snow, ice and graupel provided in the data set are converted to specific attenuation using the same method as for rainwater. Finally, the cloud water mixing ratio in each voxel is also converted to specific attenuation using the model in [15]. The synthetic attenuation field

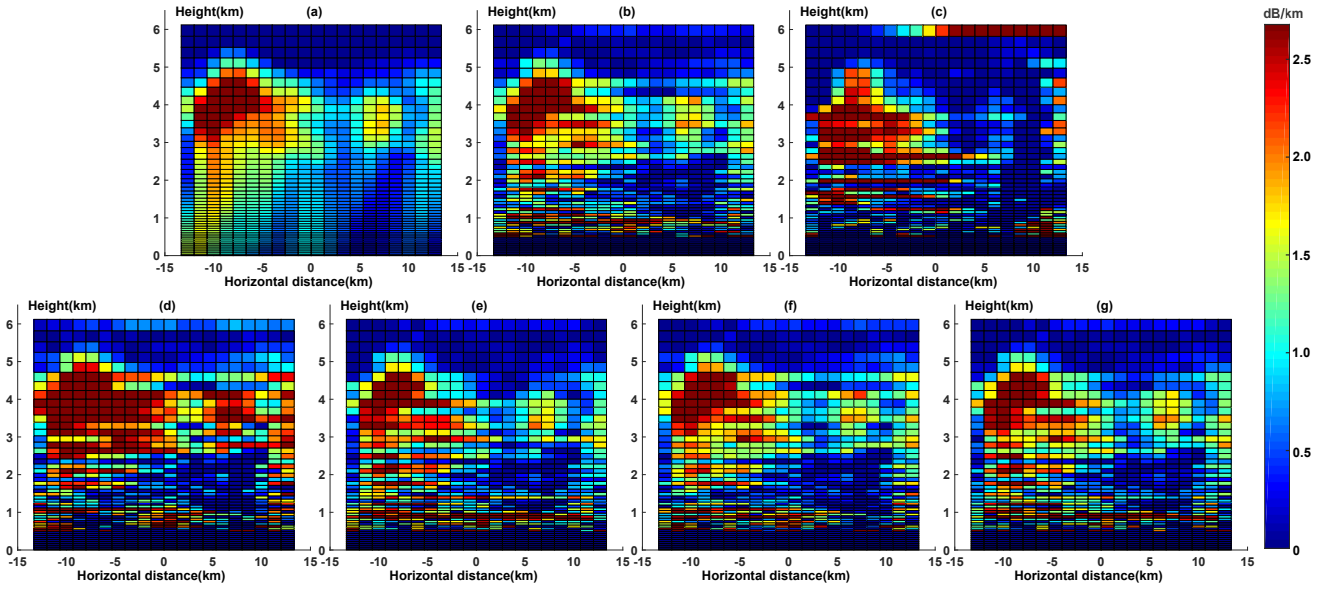

Fig. 1. A slice view of the attenuation field taken at the 9th row of the voxels. Panel (a): The original attenuation field. Panel (b): The final reconstructed field using the differential approach. Panel (c): The final reconstructed field using the non-differential approach. Panel (d - g): The reconstructed field after iterations number 1-4 using the differential approach.

is the sum of the three parts above, and our calculations show that rainwater is the major contributing part.

The same process of simulating the SNR estimation at the receivers as that used in [8] is employed. The baseline value $C(k)$ is modelled using an AR(1) process [16]:

$$C(k) = (1-\varphi)C_\infty + \varphi \cdot C(k-1) + \sqrt{1-\varphi^2} \cdot \varepsilon(k) \ ,$$

$$k = 2, 3, \cdots, M, \tag{16}$$

where φ is the correlation coefficient, C_∞ is the expectation of $C(k)$ for $k = \infty$, and $\varepsilon(k)$ is the i.i.d Gaussian model noise with zero mean and variance σ^2. Since samples are taken very close in time, the correlation coefficient φ is assumed to be high. Simulations are done for both $\varphi = 1$ ($C(k)$ is fixed) and $\varphi = 0.999$. For each receiver, $C(1)$ is chosen differently along a sine curve between 214 dB and 216 dB. Parameter C_∞ is set at 230 dB, slightly deviated from the starting value to simulate the shifting in the baseline from low to high elevation angles. For each sample, the true SNR is calculated using Eq. (1). We assume a BPSK modulated signal with a bit rate of 10 Mbps and the estimated SNR $\hat{\rho}$ is generated by adding the true SNR to a Gaussian random variable with zero mean and variance being equal to the CRLB.

It has been confirmed in [8] that the reconstruction results are not sensitive to the randomness in the receiver distribution. In the following simulations, we place 22 receivers for each row of voxels and they are equally spaced for simplicity. The non-differential method in [8] is also simulated under the same conditions for a fair comparison.

A nonnegative least-squares algorithm using an active set method [17, 18] is employed in each iteration where α is initialized to zero. The reconstructed attenuation fields at the 9th row of the voxels are shown in Fig. 1. Panel (a) is the original synthetic attenuation field, panel (d) to (g) are the interim reconstructed fields after iterations number 1-4 for a differential simulation for $\sigma = 0.8$ ($\varphi = 0.999$), and panel (b) is the final reconstruction result by averaging the 3rd and 4th iterations. The final reconstruction result under the same condition for a non-differential simulation is shown in panel (c). Comparison between (b) and (c) suggests that the improvement provided by the differential approach is significant. Due to the minimum elevation angle of the receivers (details in [8]), the bottom levels of voxels can not be reconstructed. As shown in Fig. 1(b)-(g), the simulation result confirms that the specific attenuations for the bottom 10 levels of voxels remain zero in all iterations.

We use peak signal-to-noise ratio (PSNR) [19], a measurement commonly used in image processing, to quantify the difference between the reconstructed and original fields. The PSNR for panel (b) in Fig. 1 (differential result) is 8.59 dB and for panel (c) (non-differential result) is 3.16 dB.

Multiple simulations are carried out to investigate the PSNR performance of the differential and non-differential approaches. For stochastic $C(k)$ ($\varphi = 0.999$), σ is assigned different values and the AR(1) model is simulated 50 times for both the differential and the non-differential approaches. The PSNR for the top 35 levels of voxels is recorded, the mean and standard deviation of which are shown in Fig. 2. It can be seen that the PSNR is always higher for the differential approach than for the non-differential approach. When σ takes lower values, the difference between the two approaches is greater. For instance, the mean PSNR is 8.92 dB for the differential approach and 3.30 dB for the non-differential approach when σ is 0.4. This indicates that the reconstruction is significantly better for the differential approach. For fixed $C(k)$ ($\varphi = 1$), 50 simulations suggest that the mean PSNR is 12.46 dB (also shown in Fig. 2) for the differential approach, and 11.92 dB for the non-differential approach.

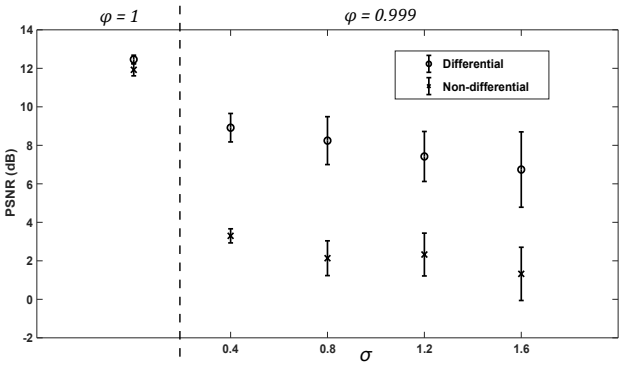

Fig. 2. PSNR for 50 independent simulations of the differential and non-differential approaches for different values of φ and σ. The error bars show the standard deviation over 50 simulations.

5. CONCLUSION

We propose a differential approach for rain field tomographic reconstruction using microwave signals from LEO satellites. This approach is based on the 3-D rain field reconstruction model which uses the estimated SNR at LEO satellite ground receivers and thus indirectly estimates the path-integrated rain attenuation of the microwave communication links. The differential approach is applied to eliminate the unknown baseline values before using least squares to reconstruct the attenuation field. Simulation results suggest that the differential approach improves the performance of the reconstruction. In particular, for stochastic baselines, the PSNR of the reconstructed rain field is significantly increased with the aid of the differential approach.

Acknowledgment

This work was supported in part by Australian Research Council Discovery Projects DP190100786.

6. REFERENCES

[1] Hagit Messer, Artem Zinevich, and Pinhas Alpert, "Environmental monitoring by wireless communication networks," *Science*, vol. 312, no. 5774, pp. 713, May 2006.

[2] Filippo Gianetti, Ruggero Reggiannini, Marco Moretti, Elisa Adirosi, Luca Baldini, Luca Facheris, Andrea Antonini, Samantha Melani, Giacomo Bacci, Antonio Petrolino, and Attilio Vaccaro, "Real-time rain rate evaluation via satellite downlink signal attenuation measurement," *Sensors*, vol. 17, no. 8, pp. 1864–1887, 2017.

[3] A. Gharanjik, Bhavani Shankar Mysore, F. Zimmer, and B. Ottersten, "Centralized rainfall estimation using carrier-to-noise of satellite communication links," *IEEE J. Sel. Area Comm.*, vol. 36, no. 5, pp. 1065–1073, 2018.

[4] C. Hakan Arslan, Kltegin Aydin, Julio V. Urbina, and Lars Dyrud, "Satellite-link attenuation measurement technique for estimating rainfall accumulation," *IEEE Trans. Geosci. Remote Sens.*, vol. 56, no. 2, pp. 681–693, 2018.

[5] Defeng Huang, Lu Xu, Xuxiang Feng, and Wanyu Wang, "A hypothesis of 3D rainfall tomography using satellite signals," *Journal of Communications and Information Networks*, vol. 1, no. 1, pp. 134–142, 2016.

[6] Avinash C. Kak and Malcolm Slaney, *Principles of Computerized Tomographic Imaging*, IEEE Press, 1988.

[7] Xi Shen, Defeng Huang, Lu Xu, and Xiaowen Tang, "Reconstruction of vertical rainfall fields using satellite communication links," in *Proc. 2017 23rd Asia-Pacific Conference on Communications (APCC)*, 2017, pp. 1–6.

[8] X. Shen, D. Huang, B. Song, C. Vincent, and R. Togneri, "3-D tomographic reconstruction of rain field using microwave signals from LEO satellites: Principle and simulation results," *IEEE Trans. Geosci. Remote Sens.*, vol. 57, no. 8, pp. 5434–5446, 2019.

[9] H. Messer and O. Sendik, "A new approach to precipitation monitoring: A critical survey of existing technologies and challenges," *IEEE Signal Process. Mag.*, vol. 32, no. 3, pp. 110–122, 2015.

[10] Takafumi Yamaji, Nobuo Kanou, and Tetsuro Itakura, "A temperature stable CMOS variable gain amplifier with 80-dB linearly controlled gain range," *IEEE J. Solid-State Circuits*, vol. 37, no. 5, pp. 553–558, 2002.

[11] International Telecommunication Union, *ITU-R P.676-6: Attenuation by atmospheric gases*, Mar. 2005.

[12] A. Tiiysiiz and F. Alagz, "Satellite mobility pattern scheme for centrical and seamless handover management in LEO satellite networks," *J. Commun. Netw.*, vol. 8, no. 4, pp. 451–460, 2006.

[13] Christian Ho, Stephen Slobin, and Kelly Gritton, *Atmospheric Noise Temperature Induced by Clouds and Other Weather Phenomena at SHF Band (1-45 GHz)*, Jet Propulsion Laboratory, 2005.

[14] John Volakis, *Antenna Engineering Handbook (4th edition)*, McGraw-Hill Professional, 2007.

[15] International Telecommunication Union, *ITU-R P.840-7: Attenuation due to clouds and fog*, Dec. 2017.

[16] G. E. P. Box, G. M. Jenkins, G. C. Reinsel, and G. M. Ljung, *Time Series Analysis: Forecasting and Control, 5th Edition*, Wiley, 2015.

[17] C. L. Lawson and R. J. Hanson, *Solving Least-Squares Problems*, Upper Saddle River, NJ: Prentice Hall, 1974.

[18] A. Bultheel and R. Cools, *The Birth of Numerical Analysis*, World Scientific, 2009.

[19] David Salomon, *Data Compression - The Complete Reference*, Springer, 2007.